Determinants of Substrate Internalization in the Distal Pocket of Dehaloperoxidase Hemoglobin of *Amphitrite ornata*[†]

Karin Nienhaus,[‡] Elena Nickel,[‡] Michael F. Davis,[§] Stefan Franzen,*[,§] and G. Ulrich Nienhaus*[,‡,||]

Institute of Biophysics, University of Ulm, Albert-Einstein-Allee 11, 89081 Ulm, Germany, Department of Chemistry, North Carolina State University, Raleigh, North Carolina 27695-8204, and Department of Physics, University of Illinois at Urbana−Champaign, 1110 West Green Street, Urbana, Illinois 61801

Received August 19, 2008; Revised Manuscript Received October 3, 2008

ABSTRACT: Dehaloperoxidase (DHP) is a small heme protein in the coelom of the terebellid polychaete *Amphitrite ornata*. It can act both as an oxygen storage protein (hemoglobin function) and as a dehaloperoxidase (peroxidase function). The X-ray structure of the ferric form shows that the phenolic substrate can bind inside the protein, which is not the case for a typical peroxidase. In the present study, we have used CO-ligated DHP to mimic the distal pocket of the peroxidase DHP and to probe under which conditions both a halophenol and a diatomic ligand can be accommodated in the distal pocket. To vary the structure of the distal pocket, we have compared wild-type DHP and mutants H55V and H55R at different pH values, using flash photolysis in the visible and FTIR spectroscopy in the CO stretching bands. The latter technique is extremely sensitive to even small structural changes in the CO environment and thus can report substrate binding in the distal pocket. Our results on wild-type DHP and its variants indicate that halophenols and a diatomic ligand can indeed simultaneously be present in the distal pocket if the distal histidine is in the low-pH conformation, in which its side chain is swung out of the distal pocket. The markedly different pH dependencies of enzyme activity and substrate binding are not consistent with the hypothesis that substrate dehalogenation occurs within the interior of DHP.

Dehaloperoxidase (DHP)[1] is the coelomic hemoglobin (Hb) of the terebellid polychaete *Amphitrite ornata*. The X-ray crystal structure reveals a protein that is composed of two identical subunits with the typical globin fold (*1*−*4*). Each DHP protomer consists of 138 amino acids so that the N- and C-termini differ in structure when compared, for example, with sperm whale myoglobin (Mb). While there are early reports of peroxidase activity in human Mb and Hb (*5, 6*), DHP is the first known Hb that plays a biological role as a peroxidase. In the presence of hydrogen peroxide (H_2O_2), DHP is capable of catalytic oxidation of 2,4,6-tribromophenol (TBP), which is secreted by marine worms such as *Thelepus crispus* and *Notomastus lobatus* that cohabit mudflats with *A. ornata* (*1, 7*−*9*). In addition, DHP can oxidize other substrates including 2,4,6-trichlorophenol (TCP) and 2,4,6-trifluorophenol (TFP), with less activity for 2,4-dichlorophenol (DCP) and still less toward monohalogenated phenols. The turnover of phenolic substrate is ∼13-fold faster than in Mb and ∼12-fold slower than in horseradish peroxidase (HRP) at pH 5 (*10*).

Early X-ray structures of DHP showed evidence for an internal site to which the substrate binds without ligating to the heme iron (*3*). This unprecedented observation led to the hypothesis that the DHP reaction mechanism is different from that of a typical peroxidase, where the phenolic substrate binds edge-on to the outside of the protein (*11*). In addition, DHP lacks both the strong hydrogen-bonding network on the proximal side and the arginine residue on the distal side required for the typical reaction mechanism as proposed by Poulos and Kraut in 1980 (*11*). Recent data indicate, however, that the dehaloperoxidase activity of DHP occurs at an exterior site (*12*). This observation seems reasonable, as the accessibility of the interior site is restricted when small ligands such as water, CN^-, CO, and O_2 are bound to the heme iron. Another study suggests, however, that a phenolic substrate can interact with a heme-bound water molecule and even displace it under certain conditions (*13*). As the interaction between the substrate and an oxo heme, which has a single oxygen atom bound to the iron, is essential for the peroxidase function and possibly even acts as a trigger to switch from the hemoglobin to the peroxidase function, the focus of this study is to elucidate the conditions under which a substrate can enter the substrate binding pocket while a ligand (here the diatomic ligand CO) is bound to the heme iron.

Association of the heme-coordinating ligand, be it dioxygen (O_2) to the hemoglobin DHP or H_2O_2 to the peroxidase DHP, might be controlled in a similar fashion in DHP and

[†] This work was supported by the Deutsche Forschungsgemeinschaft (Grant Ni 291/3) and the Fonds der Chemischen Industrie to G.U.N. and by ARO Grant 52278-LS to S.F.

* Address correspondence to these authors. G.U.N.: tel, +49 731 5023050; fax, +49 731 5023059; e-mail, uli@uiuc.edu. S.F.: tel, 919-515-8915; fax, 919-515-8920; e-mail, Stefan_Franzen@ncsu.edu.

[‡] University of Ulm.

[§] North Carolina State University.

[||] University of Illinois at Urbana−Champaign.

[1] Abbreviations: DHP, dehaloperoxidase; DHPCO, CO-ligated DHP; Mb, myoglobin; MbCO, CO-ligated Mb; TFP, 2,4,6-trifluorophenol; TBP, 2,4,6-tribromophenol; DCP, 2,6-dichlorophenol; FTIR, Fourier transform infrared; TDS, temperature derivative spectroscopy.

10.1021/bi801564r CCC: $40.75
Published on Web 11/12/2008

Mb considering their structural resemblance. Already in 1966, Perutz and Matthews suggested that fluctuations of the Mb distal histidine (H64) side chain open a direct pathway into the solvent which is used for ligand entry and exit (*14*). One might think that this hypothesis is easily tested by kinetic studies on mutants, in which H64 is replaced by a smaller residue that permanently opens the gate and thus greatly enlarges the entry rate coefficient. However, such a mutation also removes the steric hindrance exerted by the imidazole side chain at the heme iron, so that the geminate recombination barrier decreases and covalent bond formation speeds up. The competition of geminate recombination and ligand escape cannot easily be separated since both depend on the properties of the distal (E7) amino acid. The analysis is further complicated by the presence of secondary ligand docking sites C and D within the protein (*15*−*17*), which coincide with the hydrophobic protein cavities Xe4 and Xe1 (*18*−*25*). These sites enhance the probability that the ligands remain unbound inside the protein, so that they can take advantage of large-scale fluctuations that open escape pathways (*15, 26*−*29*). Despite these complications, time-resolved crystallography (*26*) and spectroscopy (*29*) experiments on a variety of mutant Mbs have provided strong support for the H64 gate mechanism in recent years.

Ligand binding studies on CO-ligated wild-type DHP (DHPCO) at cryogenic temperatures have indicated that the primary docking site B is the most frequented transient site (*30*). Only minor fractions of photolyzed ligands could be detected in other geminate sites. X-ray diffraction studies on DHP have shown conformational heterogeneity of H55 similar to that of H64 in Mb, implying that H55 might also constitute the entry/exit gate for the ligand and perhaps also for the substrate (*2, 3*). Unlike Mb, the H55 conformation in DHP appears to be governed by the ligation state of the heme iron and the presence or absence of phenolic substrate in the distal pocket. To obtain a better understanding of the role of H55 in both ligand and substrate binding, we have investigated ligand binding to and migration in CO-ligated wild-type DHP and mutants H55V and H55R. On the basis of our experience with other heme proteins, we selected the mutants for the following reasons. In H55R, the arginine side chain is protonated in the relevant pH range and oriented toward the solvent for optimal solvation of the charged guanidino group. Consequently, this mutant is expected to assume a distal pocket structure analogous to the one when H55 is swung out from the heme pocket. The Val55 side chain, by contrast, is smaller than the H55 imidazole ring. It remains in the distal pocket but renders it much more hydrophobic. Using these mutants thus allows monitoring both the steric and electrostatic effects on substrate binding.

As experimental techniques we employed flash photolysis at ambient temperature and Fourier transform infrared (FTIR) photolysis difference spectroscopy at cryogenic temperatures. Flash photolysis experiments yield information on ligand binding or hemoglobin-like properties of the mutant proteins. The FTIR technique utilizes the CO molecule as an internal probe because its stretching frequency is fine-tuned by the local electric field (*31*−*34*). Therefore, it is an ideal sensor to report on the detailed active site structure, including substrate binding in the distal pocket, as a function of temperature and pH. In the following, we will show that a close coupling exists between the bound ligand, substrate, and the distal histidine conformation.

MATERIALS AND METHODS

Ligand Binding at Ambient Temperature. CO-ligated samples were prepared in $3 \times 1 \times 1$ cm^3 glass cuvettes sealed with a rubber septum. Protein solutions at a final concentration of ~10 μM were prepared in 100 mM buffer (pH 5, potassium phosphate/citrate; pH 9, potassium phosphate) and 90%/10% glycerol/buffer, pH 5, equilibrated with 1 atm of CO to ensure anaerobic conditions, followed by reduction with a 2-fold molar excess of anaerobically prepared sodium dithionite solution. To obtain a ferrous, oxygenated DHP sample, ferric DHP was reduced with excess sodium dithionite. The excess was removed by gel filtration, which subsequently allowed the protein to bind O_2. Association rate coefficients were measured with our flash photolysis system that has been described elsewhere (*15, 16*). Up to 500 transients were averaged for each kinetic trace. Absorption changes at 436 nm were scaled according to the peak Soret absorbance of the CO-ligated species. Because the mutations are not expected to significantly change the electronic absorption properties of the heme, this procedure thus compensates for slightly different protein concentrations.

FTIR Spectroscopy. Freeze-dried DHP was dissolved in glycerol/1 M potassium phosphate or citrate/phosphate buffer (50%/50% by volume) at a final protein concentration of ~10 mM. The sample solutions were stirred under a CO atmosphere for 1 h and reduced by adding a 2-fold molar excess of an anaerobically prepared sodium dithionite solution. Subsequently, excess 2,4,6-trifluorophenol (TFP) was added for substrate-bound samples, and the solutions were stirred for another 30 min. TFP was used preferentially because of its greater solubility in aqueous solution. The pH values of the samples are quoted as measured at 290 K. The solution was centrifuged for 15 min at 5000*g* (Eppendorf centrifuge) to remove any undissolved material. Sample loading, cryogenic equipment, and photolysis setup have been described previously (*15, 30, 35*). Transmission spectra were collected in the mid-IR between 1800 and 2400 cm^{-1} with a resolution of 2 cm^{-1}, using a FTIR spectrometer (IFS 66v/S; Bruker, Karlsruhe, Germany) equipped with an InSb detector. Absorption difference spectra at 290 K in the region of the IR stretching bands of the heme-bound CO (1900−2000 cm^{-1}) were calculated from transmission spectra of CO-ligated and aquomet DHP samples according to $\Delta A = \log(I_{CO}/I_{met})$. Photolysis difference spectra were calculated from transmission spectra taken before and after photolysis for 1 s at 4 K, $\Delta A = \log(I_{dark}/I_{light})$.

Temperature Derivative Spectroscopy (TDS). To assign photoproduct bands to particular docking sites, the rebinding properties of the photoproduct species were determined using temperature derivative spectroscopy (TDS), an experimental protocol designed to study thermally activated rate processes (*36, 37*). In a first step, a nonequilibrium intermediate state is created by photolysis. Subsequently, the relaxation of the sample back to equilibrium is recorded while the temperature is ramped up linearly in time. One FTIR transmission spectrum is acquired every kelvin. Absorption difference spectra are calculated from consecutive transmission spectra;

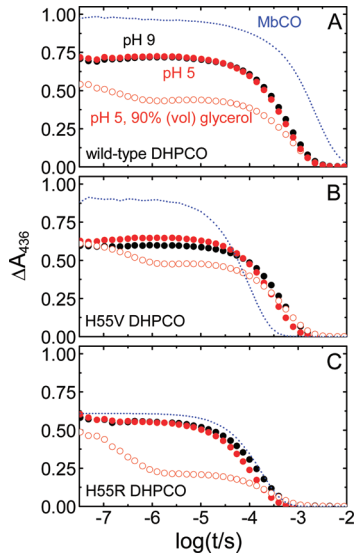

FIGURE 1: Flash photolysis kinetics of (A) wild-type DHPCO, (B) H55V DHPCO, and (C) H55R DHPCO, monitored at 436 nm and 20 °C. Solid symbols: CO rebinding in buffer. Open symbols: CO rebinding in 90%/10% (v/v) glycerol/buffer. Red/black symbols: pH 5.0/9.0. Kinetic traces of MbCO in buffer, pH 8, are included as blue lines.

they reveal changes within a temperature interval of 1 K that may arise not only from recombination but also from intrinsic peak shifts and absorbance changes due to ligand dynamics (*31, 32, 37*). FTIR-TDS data are presented as contour plots of the absorbance changes on a surface spanned by temperature and wavenumber. Black and red lines indicate an absorbance increase and decrease, respectively. Contours are spaced logarithmically to enhance small-amplitude features.

RESULTS

Ligand Binding at 290 K. To obtain insight into the ligand binding (hemoglobin function) properties at ambient temperature, flash photolysis experiments were performed on the CO-ligated wild-type, H55R, and H55V samples. The kinetic traces showing the decay of the deligated pentacoordinate ferrous species formed upon photodissociation of CO molecules are depicted in Figure 1; traces of the corresponding sperm whale MbCO samples have been included for comparison. The amplitudes at the earliest times were scaled according to the absorption difference between the steady-state CO and deoxy spectra at 436 nm of the respective samples and then normalized to 1, so that the data in Figure 1 indicate the fraction of ligands that have not rebound within time t after photolysis. The bimolecular process was fitted with an exponential to obtain the (pseudo-first-order) apparent rate coefficient, λ_S, for bimolecular CO binding from the solvent. For the data measured in buffer, we have converted the λ_S values to second-order rate coefficients, k_{on}, by using [CO] = 1000 μM (Table 1).

In buffer solution, the geminately rebinding fraction in DHPCO (pH 5 and 9) amounts to ~30%, as compared to only 4% in MbCO (*38*). Bimolecular CO and O_2 binding to wild-type DHP are ~3-fold faster than to Mb (Figure 1A, Table 1). A small increase in the association rate coefficient is observed upon lowering the pH (Figure 1A). The comparison of the corresponding Mb and DHP mutants

Table 1: Association Rate Coefficients of Bimolecular CO Binding to Wild-Type and Mutant DHP and Mb Samples

	k_{on} (μM^{-1} s^{-1})			
sample	CO, pH 5	CO, pH 9	CO, pH 8	O_2, pH 7
wild-type DHPCO	1.7	1.5		37
H55V DHPCO	2.9	1.9		
H55R DHPCO	8.5	5.8		
Mb			0.51	16
H64L Mb			7.0	
H64R Mb			5.7[a]	

[a] Data taken from ref *63*.

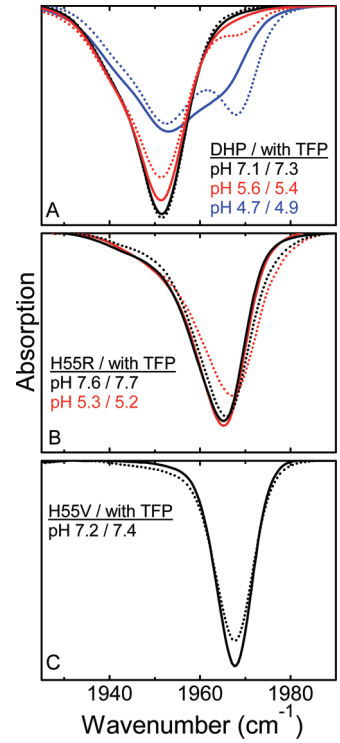

FIGURE 2: Absorption difference spectra of CO-ligated DHP samples at 290 K, referenced to met DHP. (A) Wild-type DHPCO. (B) H55R DHPCO. (C) H55V DHPCO. All spectra have been scaled to the same area. Solid lines: CO-ligated protein. Dotted lines: CO-ligated protein with TFP added.

shows that CO binding to H55V DHP is slower than to H64V Mb (Figure 1B), whereas H55R DHP and H64R Mb have essentially identical CO association rate coefficients (Figure 1C). Overall, the variation of the association kinetics among the DHP mutant samples is rather small.

Remarkably, no change in the kinetics of CO rebinding to DHP is observed in the more viscous 75%/25% glycerol/buffer solutions (*30*). In 90% glycerol, however, geminate rebinding is further enhanced for all three DHP samples. The geminate process, which is faster than the observation time window of our flash photolysis system for aqueous samples, is clearly seen out to the microsecond range in 90% glycerol. In mutant H55R, ~80% of the ligands rebind from within the protein in the high-viscosity solvents, whereas the geminate fractions are 56% and 52% for wild-type DHP and H55V. However, the bimolecular association rate coefficients are essentially unchanged in 90% glycerol.

Structural Heterogeneity of the DHP Active Site at 290 K. Figure 2 displays FTIR absorption difference spectra of the CO-ligated proteins in the region of the CO stretching frequency, measured at 290 K and referenced to aquomet

Table 2: Stretching Frequencies of the Absorbance Bands of Heme-Bound CO in DHPCO Mutants, Determined at 290 and 4 K[a]

		ν(heme-bound CO) (cm^{-1})		ν(photolyzed CO) (cm^{-1})
sample	A state	290 K	4 K	4 K
wild-type DHP	A_3	1940	1941	2118, 2135
	A_1	1951	1941	2124, 2128
	A_0	1964	1965	2126
	A_s	1969	1972	2122, 2126
H55R		1940	1956	
		1953	1964	
		1965	1972	
		1967		
H55V		1954	1954	
		1967	1963	
			1970	

[a] Underlined values: TFP was added to the samples.

DHP. Multiple CO stretching bands are observed that, for MbCO and several other heme proteins, are known to arise from different local electrostatic environments of the heme-bound CO (*39*−*44*). In Mb, the distal histidine His-64 side chain is positioned in various ways so as to produce different electrostatic interactions with the bound CO ligand (*15, 45, 46*). To compensate for slight differences in sample concentration and path length, all spectra were scaled to equal areas and fitted with Gaussian distributions to determine peak positions and fractional areas; peak positions are compiled in Table 2.

The absorption spectrum of wild-type DHPCO (pH 7.1) displays a dominant band at 1951 cm^{-1} (Figure 2A) (*30*). A shoulder at 1940 cm^{-1} can be fitted by an additional band with 19% of the total area (Figure 3A). By analogy with MbCO, we will denote these bands as A_1 ($\nu = 1951$ cm^{-1}) and A_3 ($\nu = 1940$ cm^{-1}). Compared with Mb ($\nu(A_1) = 1945$ cm^{-1}, $\nu(A_3) = 1930$ cm^{-1} (*15, 47, 48*)), the A_1 and A_3 bands both have slightly higher stretching frequencies. The equilibrium between the A_1 and A_3 conformations at pH 7.1 does not depend on sodium chloride concentration in the buffer (0−1.5 M), on glycerol content, or on the presence of substrate (here TFP). However, as shown in Figure 3, the A_3 percentage of the total spectral area increases from 19% to 25% as the sample is cooled from 290 to 4 K. In analogy to Mb, we suggest that A_1 and A_3 represent two different conformations, in which the H55 side chain is in the distal pocket and establishes a hydrogen-bonding interaction with the bound ligand. The observation that both frequencies are upshifted as compared with MbCO implies that the interaction with H55 is weaker, possibly because of a larger distance between the CO and the imidazole.

Upon lowering the pH, an additional absorption band at 1964 cm^{-1} appears, the fractional area of which increases with decreasing pH (Figure 2A). This dependence suggests that the band is caused by protonation of H55 (*39, 45*). In analogy to Mb, we assign this band to the A_0 conformation, in which the protonated H55 side chain is rotated toward the solvent for better charge solvation (*45*). The frequency shift is caused by the loss of the hydrogen bond to the CO. The N−H···OC hydrogen bonding of the distal H55 is removed (*34*). In Figure 3D, we have plotted the fraction of A_0 in DHPCO as a function of pH. Unfortunately, the protein becomes unstable below pH 4.5 so that we were not able to follow the pH dependence over a wider range. A fit of these

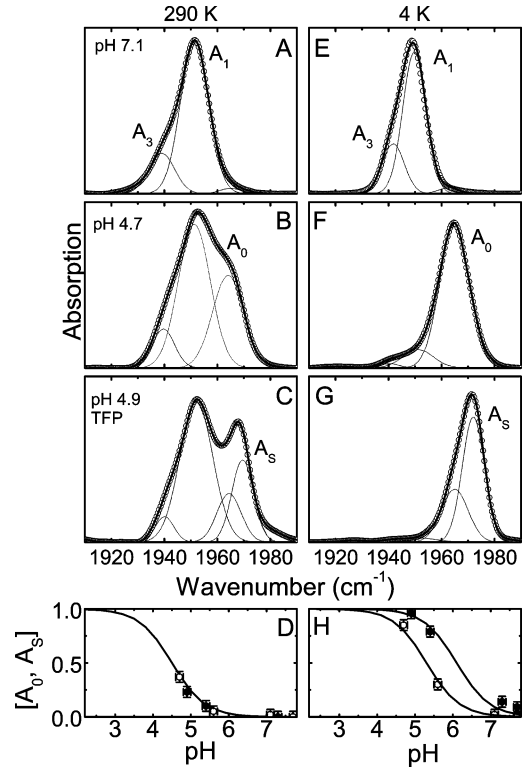

FIGURE 3: Absorption difference spectra of CO-ligated DHP samples at (A, B, C) 290 K and (E, F, G) at 4 K. The data (open circles) were fitted with Gaussians (thin lines), with the sum given by the bold line. Fractions of A_0 (open symbols) and A_S (closed symbols) in wild-type DHPCO as a function of pH at (D) 290 K and (H) 4 K. Lines represent titration curves according to the Henderson−Hasselbalch relation.

data with the Henderson−Hasselbalch relation indicates that protonation of H55 at 290 K and the concomitant appearance of A_0 occur with $pK_a = 4.5$ (Figure 3D, open symbols). This value is identical to that of H64 in wild-type MbCO (*49*).

To provide additional support for the A_0 assignment, we have also collected FTIR spectra of mutants H55R at pH 5.3 and 7.6 and H55V at pH 7.2 (Figure 2B,C). The absorption signal of H55R has its maximum at 1965 cm^{-1}. Broadening of the peak toward lower wavenumbers can be described by additional bands at 1940 and 1953 cm^{-1}. The R55 side chain, with its pK_a of ∼12, is positively charged under our experimental conditions. If it resided in the distal pocket, it should cause a pronounced shift of the CO frequency to a value significantly lower than the wild-type A_1 frequency of 1951 cm^{-1} (*41*). Consequently, we conclude that the guanidino moiety of R55 is not resident in the hydrophobic distal pocket but rather oriented toward the solvent. The frequency of 1965 cm^{-1} thus corresponds to an A_0-like, open conformation, similar to the wild-type protein with a protonated H55. H55V has a rather narrow CO stretching band at 1967 cm^{-1}, close to the frequency of the MbCO H64V at 1968 cm^{-1} (*39, 40*). In this case, the N−H···OC hydrogen bonding donated by the distal H55 is removed by mutagenesis; the small, hydrophobic V55 side chain, however, is still inside the pocket (*34*).

The addition of TFP to wild-type DHPCO at pH 7.3 (Figure 2A, dotted lines) has essentially no influence on the infrared absorption spectrum at 290 K. The same holds true for pH 10.8 (data not shown). At pH 5.4, a minor band is seen at 1968 cm^{-1}, which we denote as A_S. The subscript

"S" refers to a conformation with a phenolic substrate present in the distal pocket. The amplitude of the A_S band increases markedly when the sample pH is lowered to 4.9 (Figure 2A). The increase in stretching frequency of the A_S band relative to A_0 indicates that the influence of the positive partial charge due to the N−H···OC interaction of H55 is absent because the distal H55 is in the open conformation, and an additional negative partial charge has been introduced in the vicinity of the heme-bound ligand. We suggest that the charge originates from the π-electron system of the aromatic substrate, which has entered the distal pocket. The pH dependence of the A_S population (substrate TFP) appears to be similar to that of A_0 (Figure 3D, closed symbols). This result strongly suggests that only DHP molecules in the A_0 conformation can accommodate a substrate and that stabilizing effects on A_0 due to TFP binding are negligible at ambient temperature.

The distal pocket of the H55R mutant is expected to be predominantly in the open conformation at pH 7.6 and 5.3, since R55 is charged and removed from the distal pocket, as judged from its CO stretching band at 1965 cm^{-1}. Therefore, one would expect a full occupancy of the pocket with a phenolic substrate if its binding were only governed by the protein conformation. However, addition of TFP to mutant H55R at pH 7.7 induces only a minimal change in the spectrum. At pH 5.2, however, the CO absorption maximum shifts from 1965 to 1968 cm^{-1} (Figure 2B). A fit of these spectra with Gaussian distributions shows that the broadening can be attributed to an A_S band at 1967 cm^{-1} with 20% (pH 7.7) and 67% (pH 5.2) of the total area. If one assumes that only A_0 can accommodate the substrate, its fractional occupancy with substrate amounts to ~25% (pH 7.7) and ~90% (pH 5.3). This pH dependence most likely reflects the protonation state of the substrate. Considering a pK_a of 7.1 for TFP at 290 K (Supporting Information), the data imply that preferentially neutral TFP molecules enter the distal pocket. HRP was also shown to have a higher affinity for neutral phenols (*50*).

The spectrum of H55V DHPCO does not reveal any noticeable changes upon addition of TFP (Figure 2C). Apparently, introduction of the hydrophobic V55 side chain completely suppresses substrate entry into the distal pocket, either because of steric hindrance or increased hydrophobicity. The same negative result was obtained with DCP (data not shown).

Structural Heterogeneity of the DHP Active Site at 4 K. In Figure 4, we compare photolysis-induced absorption difference spectra of wild-type, H55R, and H55V DHPCO at 4 K. The bands associated with heme-bound CO are plotted with a negative absorption because these features are missing after photolysis, whereas the bands representing the photodissociated CO appear with a positive absorption. The overall spectral area of the photoproduct bands is ~20× smaller than that of the A state bands. For better comparison, we have scaled all spectra to identical maximum amplitudes. The absorption bands of heme-bound CO are slightly shifted compared to the bands at 290 K. The peak positions are included in Table 2.

The temperature change has noticeably shifted the fractional populations of the distal histidine conformations in wild-type DHPCO at a given pH (compare the spectra in the left and right columns in Figure 3 that were taken on

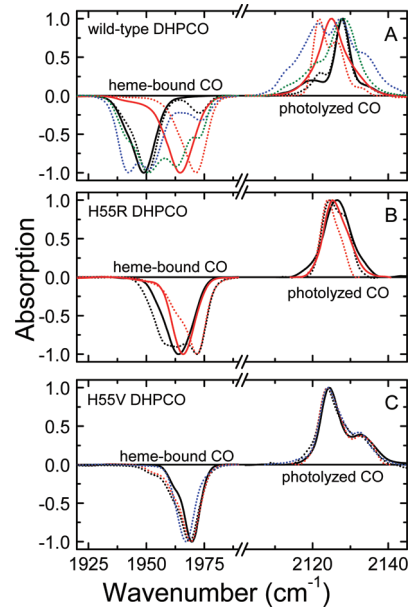

FIGURE 4: Photolysis difference spectra of DHPCO samples, calculated from transmission spectra taken before and after 1 s illumination at 4 K. (A) Wild-type DHPCO. (B) H55R DHPCO. (C) H55V DHPCO. All spectra were scaled to the same maximal amplitude. Solid and dotted lines refer to samples without and with substrate added. Black: TFP, pH ~7. Red: TFP, pH ~5. Blue: DCP, pH ~7. Green: TBP, pH ~5.

identical samples). The transition occurs gradually between 290 and 200 K (Supporting Information). In this temperature region, the protein is still flexible, and therefore, large-scale conformational changes are possible (*51, 52*). At 4 K, the protonation of H55 is described by an apparent pK_a = 5.3 (Figure 3D). This result reflects the fact that temperature can have a marked effect on the protonation of amino acids, here H55 (*53*). Another prominent example is MbCO, for which cooling results in a shift of the protonation equilibrium of H64 corresponding to an apparent pK_a increase of ~1.2 pH units in 75%/25% (by volume) glycerol/buffer solution (*39*).

In the presence of TFP, the A_S band at 1972 cm^{-1} is clearly visible even at pH 7.3 (Figure 4A), in contrast to the spectrum at 290 K (Figure 2A). The A_S band is also displayed in the spectrum of wild-type DHPCO after addition of DCP (blue line in Figure 4A) and TBP (green line in Figure 4A). The apparent pK_a for TFP binding has shifted from 4.5 to 6.2 and thus 0.9 pH unit more than that of H55 (compare Figure 3D and 3H). This finding implies that, upon cooling from ambient to cryogenic temperatures, the A_0 conformation is stabilized by a few kilojoules per mole by TFP binding. On the basis of the data obtained with mutant H55R at 290 K, we have proposed that only neutral substrate molecules enter the distal pocket. We have verified that the apparent pK_a of TFP increases upon cooling (Supporting Information) and, therefore, the bound TFP molecules are neutral also at 4 K.

Photolysis difference spectra of H55R DHPCO are plotted in Figure 4B. The spectrum at pH 7.6 can be modeled with two Gaussian lines at 1959 and 1966 cm^{-1}, whereas a single band at 1966 cm^{-1} suffices to describe the spectrum at pH 5.3. Upon addition of TFP, the A_S band (ν = 1972 cm^{-1}) is clearly resolved at both pH values (Figure 4B). Additionally, the spectrum of the pH 7.7 sample is substantially broadened toward lower wavenumbers.

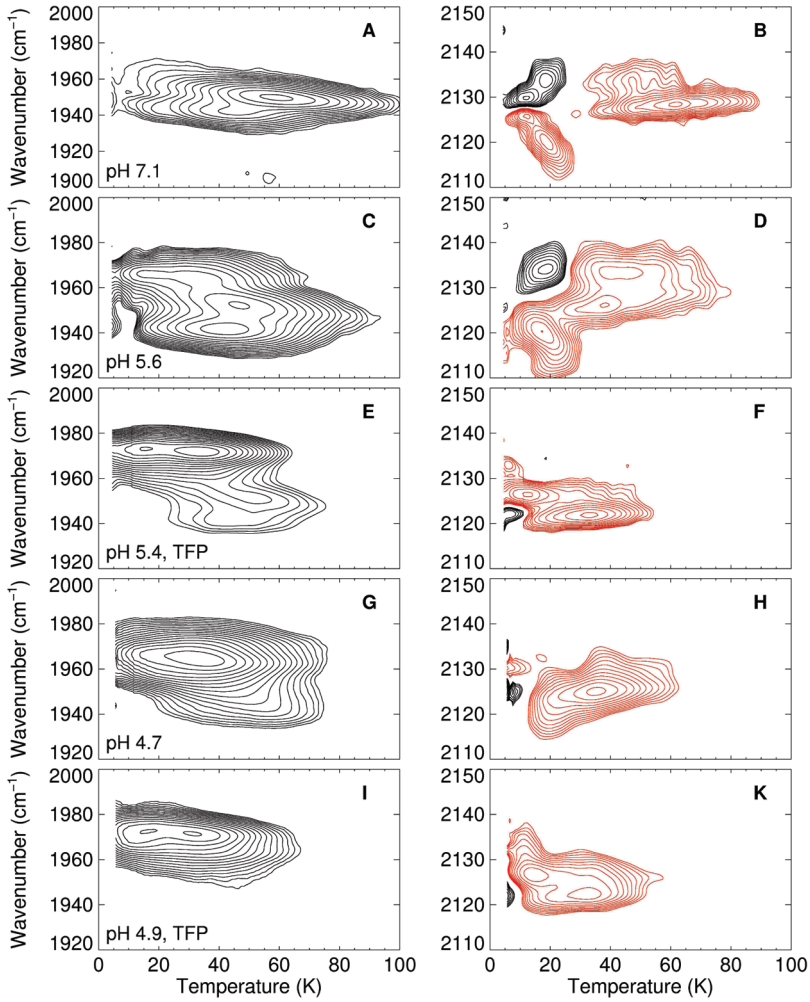

FIGURE 5: TDS contour maps of different wild-type DHPCO samples. Data were taken after 1 s illumination at 4 K. Left column: Absorption changes in the bands of heme-bound CO. Right column: Absorption changes in the photoproduct bands. Contours are spaced logarithmically; black and red lines represent increasing and decreasing absorption, respectively.

The absorption spectra of H55V DHPCO at 4 K can be fitted with two bands at 1962 and 1970 cm^{-1} (Figure 4C). In contrast to wild-type and H55R DHPCO, we did not detect any A_S-like band with a frequency higher than that of A_0 at 4 K. Instead, addition of TFP and DCP leads to an increase of the shoulder at 1962 cm^{-1} and to a new band at 1954 cm^{-1}.

CO at the Primary Docking Site B. In an earlier study, we already showed that 1 s illumination of wild-type DHPCO at 4 K results in ligand migration to a primary docking site B (*30*). In analogy to Mb, this site is expected to be in close proximity to the heme iron (*33, 54*−*59*). The stretching frequency of the photodissociated CO molecule is fine-tuned by the local electric field at the docking site, which is governed by different structures of the distal pocket as well as binding of the phenolic substrate. The photoproduct spectra can thus provide a second means to probe substrate binding.

The photolysis difference spectra in Figure 4 reveal multiple stretching bands in the spectral range of photodissociated CO between 2100 and 2150 cm^{-1} that overlap extensively. A priori, an assignment of the bands is not feasible because they may represent ligands trapped at the same site but in different protein subconformations, in different orientations within one site, or even at different sites. To disentangle the photoproduct bands and associate them with particular subconformations, TDS measurements were started immediately after the 1 s illumination at 4 K. The temperature ramp ensures that rebinding occurs sequentially with respect to the temperature at which the different processes become activated. In the left (right) column of Figure 5, we have plotted the absorption changes in the bands of heme-bound (photolyzed) CO. Black (red) lines indicate that the absorption increases (decreases) due to rebinding.

Since substrate binding occurs preferentially at low pH, we present contour plots of wild-type DHPCO samples at pH 5.6 and 4.7 both with and without TFP. The contour maps of wild-type DHPCO (pH 7.1), which were published previously (*30*), are included in panels A and B of Figure 5 as reference data. From Figure 5A, it is apparent that rebinding in A_1 peaks at 60 K. At the same temperature, the absorption loss in the photoproduct band at 2128 cm^{-1} is maximal, indicating that this band represents photolyzed ligands at site B in A_1 molecules (Figure 5B). Below ~30 K, we observe a mirror image of black and red contours. These contours indicate that the photoproduct band at 2128 cm^{-1} gains amplitude at the expense of the band at 2124 cm^{-1}. This exchange feature has been observed for many heme proteins and represents ligand reorientation at docking site B between two opposite orientations. The doublet of bands at 2124 and 2128 cm^{-1} arises because the local electric field at the docking site induces a shift of the CO stretching

band (vibrational Stark effect) that depends on the orientation of the CO with respect to the electric field (*33, 54, 55*). Detailed theoretical analyses suggest that the bands at 2124 and 2128 cm^{-1} are associated with the Fe···OC and Fe···CO orientations, respectively (*33, 55*).

In the TDS maps of wild-type DHPCO at pH 5.6, the features related to A_3 dominate. Maximal rebinding in A_3 occurs at 40 K (Figure 5C). The corresponding photoproduct map (Figure 5D) shows an exchange between the bands at 2118 and 2135 cm^{-1} below 30 K, which is also displayed in Figure 5B, and rebinding from B_{2135} at 40 K. Thus, the two photoproduct bands again appear to constitute a doublet arising from vibrational Stark splitting; it is assigned to $B(A_3)$. We note that $B(A_3)$ in MbCO is also associated with a doublet of bands that is more widely split than that of $B(A_1)$ (*60*). In the TDS maps of the wild-type DHPCO sample at pH 4.7, A_0 is the dominant species (Figure 5G). Photodissociated ligands are represented by a single photoproduct band at 2126 cm^{-1} although both CO orientations are likely to occur. A single photoproduct band has also been observed in Mb mutant H64L (*33*). These findings suggest that the interaction between the H55 side chain and the CO ligand at site B is the main determinant of the Stark splitting. This interpretation is supported by the photoproduct spectrum of H55R, which shows a rather broad feature, with only little structure (Figure 4B). In this context, it seems surprising that the photoproduct spectrum of H55V DHPCO displays a clear doublet of bands (Figure 5C). A comparison of the TDS experiments following 1 s illumination at 4 K and slow cooling under continuous illumination shows, however, that the high-frequency photoproduct band is, in fact, a doublet which represents CO ligands at a secondary docking site (Supporting Information).

After TFP has been added, the A_S band appears. CO rebinding in A_S molecules occurs in two distinct steps at 15 and 32 K, respectively (Figure 5E,I). The corresponding photoproduct maps in panels F and K of Figure 5 show a concomitant loss in photoproduct bands at 2122 and 2126 cm^{-1}, which are consequently assigned as $B(A_S)$. Ligand reorientation is not resolved, however, suggesting that the bulky substrate prevents ligand rotation in site B so that they may rebind directly at the heme iron from either position.

DISCUSSION

The role played by H55 in the distal pocket of DHP is strongly analogous to that of the distal histidine of Mb. DHP, however, has the additional feature that a phenolic substrate can enter the distal pocket. We have investigated the conditions for substrate entry using FTIR spectroscopy, with the CO vibration as a reporter of the electrostatic environment at the active site. The distal pocket of Mb is optimized for O_2 binding; the hydrogen bond donated to the bound O_2 by the distal H64 discriminates against the binding of CO. Different orientations of the distal histidine cause conformational heterogeneity at the active site of MbCO, and three major conformations, denoted as A_0, A_1, and A_3, can be associated with the CO stretching bands at 1966, 1945, and 1930 cm^{-1} (*15, 36, 47*). The observed CO frequency dispersion is caused by electrostatic interactions, mainly between the CO dipole and the imidazole side chain of H64 (*39, 40, 49*). In the high-pH conformations A_1 and A_3, the imidazole is neutral and resides in the distal pocket. The X-ray structure at 1.2 Å resolution suggests that it is located more deeply in the heme pocket in A_3 than in A_1 (*46*). In the low-pH conformation A_0, the imidazole is protonated (pK_a = 4.5 (*49*)) and rotated toward the solvent for better screening of its charge (*45*).

Our extensive knowledge of the relationship between structure and spectra in MbCO, including many mutants, sets the stage for the interpretation of the present results with DHP. The FTIR difference spectra of DHPCO also show up to three stretching bands of the heme-bound CO that are associated with specific active site conformations. In the first X-ray structures of the ferric form at pH 6.5 collected at ambient temperature, the H55 side chain was resolved both inside and outside of the distal pocket, and the heme group was shifted ~1.5 Å further into the protein as compared to Mb (*3*). As a consequence, the distance between H55 in the closed conformation and the heme iron is 1.2 Å larger than in Mb in the room temperature X-ray structure (*3*). The greater Fe−Nϵ distance implies a weaker hydrogen-bonding interaction between the imidazole side chain and a heme-bound diatomic ligand, which results in an increased frequency of the stretching band of A_1 in DHPCO (1951 cm^{-1}) compared to MbCO (1945 cm^{-1}). The recent X-ray structure analysis of aquomet DHP at pH 6.5 and 100 K has shown a closed conformation, in which the H55 side chain is located 0.75 Å closer to the heme than in the initial structure and, therefore, within hydrogen-bonding distance to either bound H_2O or O_2 (*2*). It is logical to extend this reasoning to bound CO and propose that the closed conformation observed at 100 K is related to the A_3 stretching band, while the one at room temperature is associated with the A_1 stretching band. This assignment is supported by the finding that the fraction of A_3 increases slightly upon cooling. The open conformation, observed in the room temperature X-ray crystal structure of LaCount et al. (*3*), is represented by A_0. The pH dependence of the CO band areas implies that the H55 side chain is protonated in A_0 and therefore rotated out of the hydrophobic pocket.

The A substate bands in MbCO have markedly different ligand binding kinetics (*48, 61*). Upon dissociation of a ligand from the Mb iron at pH 9, where only A_1 and A_3 are present, the H64 side chain moves slightly deeper into the distal pocket and increases the steric hindrance at the heme iron against immediate geminate rebinding, leading to efficient ligand escape. Lowering the pH increases the fraction of Mb molecules with a protonated His side chain (*49*). The side chain rotates away from the heme iron and no longer blocks ligand access (*45*), and we thus observe less efficient ligand escape and faster ligand association at low pH (*62*). The same effect is obtained by replacing H64 with small aliphatic amino acids, which causes the association rate coefficients to increase up to 40-fold (*63*).

In DHP, the corresponding H55 side chain is further away from the heme iron than in Mb and is, therefore, expected to have a smaller effect on the ligand binding kinetics. Figure 1 shows only minor changes in the association kinetics of DHP upon lowering the pH or replacing H55, which suggests that H55 plays a relatively small role in controlling ligand rebinding kinetics. This observation might imply that the importance of the O_2 binding function is different from Mb. Specifically, the discrimination against CO would be ex-

pected to be weaker. These differences may be associated with the fact that DHP has a dual function, but they may also depend on the specific environmental effects in the benthic ecosystem where *A. ornata* is found.

Based on studies of the ability of *A. ornata* to dehalogenate the common repellent 2,4,6-TBP, it has been concluded that dehalogenation is an important secondary physiological function of DHP. As the initial X-ray diffraction data showed the substrate analogue *p*-iodophenol inside the distal pocket (*3*), DHP was assumed to process its substrate internally, in contrast to typical peroxidases such as HRP. This mechanism would require the substrate to be accommodated in the distal heme pocket, with either H_2O_2 or the single oxygen atom bound to the heme iron at the same time. To model this scenario, we have probed substrate binding in the presence of heme-bound CO. After adding TFP to a CO-ligated sample, a new IR stretching band A_S was observed at low pH, indicating that the local environment of the CO has changed and that the substrate has indeed entered the pocket. The area of the A_S band increases upon decreasing the pH, with a pK_a of 4.5. The observation of an identical pK_a for the appearance of the A_0 conformation strongly suggests that *only* the open conformation of DHPCO can accommodate a substrate molecule inside the distal pocket. This hypothesis is further corroborated by the substrate binding behavior of mutant DHPCO H55R (Figure 4B), which is in the open conformation at all pH values that are relevant here. The occupancy is not determined by the protein conformation, but rather by the protonation state of the substrate. The higher occupancy at low pH indicates that mainly neutral substrate molecules bind in its distal pocket. Remarkably, H55V DHPCO does not bind any phenolic substrate because of steric conflicts or hydrophobicity. We have further confirmed that binding of TFP in the A_0 conformation of MbCO does not occur (data not shown). In contrast to DHPCO, the MbCO sample did not exhibit any TFP-related A_S absorption band.

If only the open conformation can accommodate the substrate, and the substrate has to be within the active site to be dehalogenated, the peroxidase activity should increase upon lowering the pH. pH-dependent activity studies on DHP have shown, however, that the addition of H_2O_2 at pH < 6.5 leads to significant heme degradation both with and without substrate present and thus to very low or even no activity (*12*). At pH >6.5, H_2O_2 interacts with the iron and forms the typical, catalytically active oxo species as required by the Poulos−Kraut mechanism. One could now argue that, in the open conformation, the distance between H55 and heme-bound H_2O_2 is too large for H55 to act as an acid/base catalyst (*11*). In Mb mutant L29H-H64L, where the histidine−iron distance is 6.6 Å, peroxidase activity is totally lost, whereas it is ~11-fold enhanced in double mutant F43H-H64L; in the latter protein, H43 is 5.4 Å away from the ferric iron and thus at a distance typical for a peroxidase (*64*). In this scenario, one would expect the greatest activity at pH values below the pK_a of the substrate to at least maximize the fraction of neutral substrate. However, the enzyme activity is maximal at pH 7.5, which is above the pK_a of the physiological substrate, TBP (*12*). At pH > 8.5, DHP was found to be devoid of any peroxidase activity because of the formation of the methydroxy adduct. Thus, the maximum activity of DHP does not coincide with maximal substrate binding in the distal pocket. We conclude that the phenomenon of substrate binding in the distal pocket is not required for dehaloperoxidase function but could possibly play a role in allostery, in function switching, or perhaps in an alternative function that has not yet been discovered.

CONCLUSION

The FTIR absorption spectra indicate unambiguously that there is sufficient room in the distal cavity of DHP for both a diatomic ligand and a phenolic substrate, provided that the distal histidine is in the open conformation. This finding suggests that the observation of substrate in the DHP distal pocket is not simply an artifact of the X-ray crystal structure. However, the pH dependence of the effect contributes to the evidence that the distal pocket is not the active site for dehaloperoxidase activity.

SUPPORTING INFORMATION AVAILABLE

Temperature-dependent spectra of DHPCO, pH 4.7, optical spectra of TFP, and TDS contour maps of H55V DHPCO. This material is available free of charge via the Internet at http://pubs.acs.org.

REFERENCES

1. Roach, M. P., Chen, Y. P., Woodin, S. A., Lincoln, D. E., Lovell, C. R., and Dawson, J. H. (1997) Notomastus lobatus chloroperoxidase and Amphitrite ornata dehaloperoxidase both contain histidine as their proximal heme iron ligand. *Biochemistry 36*, 2197–2202.
2. de Serrano, V., Chen, Z., Davis, M. F., and Franzen, S. (2007) X-ray crystal structural analysis of the binding site in the ferric and oxyferrous forms of the recombinant heme dehaloperoxidase cloned from Amphitrite ornata. *Acta Crystallogr., Sect. D: Biol. Crystallogr. 63*, 1094–1101.
3. LaCount, M. W., Zhang, E., Chen, Y. P., Han, K., Whitton, M. M., Lincoln, D. E., Woodin, S. A., and Lebioda, L. (2000) The crystal structure and amino acid sequence of dehaloperoxidase from Amphitrite ornata indicate common ancestry with globins. *J. Biol. Chem. 275*, 18712–18716.
4. Franzen, S., Roach, M. P., Chen, Y.-P., Dyer, R. B., Woodruff, W. H., and Dawson, J. H. (1998) The unusual reactivities of Amphitrite ornata dehaloperoxidase and Notomastus lobatus chloroperoxidase do not arise from a histidine imidazolate proximal heme iron ligand. *J. Am. Chem. Soc. 120*, 4658–4661.
5. George, P., and Irvine, D. H. (1951) Reaction of methmyoglobin with hydrogen peroxide. *Nature 168*, 164–165.
6. George, P., Lyster, R. L., and Beetlestone, J. (1961) The reaction of ferrimyoglobin with phenol. *J. Biol. Chem. 236*, 3246–3251.
7. Chen, Y. P., Woodin, S. A., Lincoln, D. E., and Lovell, C. R. (1996) An unusual dehalogenating peroxidase from the marine terebellid polychaete Amphitrite ornata. *J. Biol. Chem. 271*, 4609–4612.
8. Chen, Y. P., Lincoln, D. E., Woodin, S. A., and Lovell, C. R. (1991) Purification and properties of a unique flavin-containing chloroperoxidase from the capitellid polychaete Notomastus lobatus. *J. Biol. Chem. 266*, 23909–23915.
9. Woodin, S. A., Marinelli, R. L., and Lincoln, D. E. (1993) Biogenic brominated aromatic compounds and recruitment of infauna, *J. Chem. Ecol. 19*, 517–530.
10. Belyea, J., Godek, M., Davis, M. F., Gilvey, L. B., Sit, T. L., Lommel, S. A., and Franzen, S. (2005) Enzyme function of the globin dehaloperoxidase from Amphitrite ornata is activated by substrate binding. *Biochemistry 44*, 15637–15644.
11. Poulos, T. L., and Kraut, J. (1980) The stereochemistry of peroxidase catalysis. *J. Biol. Chem. 255*, 8199–8205.
12. Franzen, S., Gilvey, L. B., and Belyea, J. L. (2007) The pH dependence of the activity of dehaloperoxidase from Amphitrite ornata. *Biochim. Biophys. Acta 1774*, 121–130.
13. Smirnova, T. I., Weber, R. T., Davis, M. F., and Franzen, S. (2008) Substrate binding triggers a switch in the iron coordination in dehaloperoxidase from Amphitrite ornata: HYSCORE experiments. *J. Am. Chem. Soc. 130*, 2128–2129.

14. Perutz, M. F., and Mathews, F. S. (1966) An x-ray study of azide methaemoglobin. *J. Mol. Biol. 21*, 199–202.
15. Nienhaus, K., Deng, P., Kriegl, J. M., and Nienhaus, G. U. (2003) Structural dynamics of myoglobin: The effect of internal cavities on ligand migration and binding. *Biochemistry 42*, 9647–9658.
16. Nienhaus, K., Deng, P., Kriegl, J. M., and Nienhaus, G. U. (2003) Structural dynamics of myoglobin: spectroscopic and structural characterization of ligand docking sites in myoglobin mutant L29W. *Biochemistry 42*, 9633–9646.
17. Nienhaus, G. U., and Nienhaus, K. (2002) Infrared study of carbon monoxide migration among internal cavities of myoglobin mutant L29W. *J. Biol. Phys. 28*, 163–172.
18. Tilton, R. F., Jr., Kuntz, I. D., Jr., and Petsko, G. A. (1984) Cavities in proteins: structure of a metmyoglobin-xenon complex solved to 1.9 Å. *Biochemistry 23*, 2849–2857.
19. Ostermann, A., Waschipky, R., Parak, F. G., and Nienhaus, G. U. (2000) Ligand binding and conformational motions in myoglobin. *Nature 404*, 205–208.
20. Srajer, V., Ren, Z., Teng, T. Y., Schmidt, M., Ursby, T., Bourgeois, D., Pradervand, C., Schildkamp, W., Wulff, M., and Moffat, K. (2001) Protein conformational relaxation and ligand migration in myoglobin: a nanosecond to millisecond molecular movie from time-resolved Laue x-ray diffraction. *Biochemistry 40*, 13802–13815.
21. Bourgeois, D., Vallone, B., Schotte, F., Arcovito, A., Miele, A. E., Sciara, G., Wulff, M., Anfinrud, P., and Brunori, M. (2003) Complex landscape of protein structural dynamics unveiled by nanosecond Laue crystallography. *Proc. Natl. Acad. Sci. U.S.A. 100*, 8704–8709.
22. Chu, K., Vojtechovsky, J., McMahon, B. H., Sweet, R. M., Berendzen, J., and Schlichting, I. (2000) Structure of a ligand-binding intermediate in wild-type carbonmonoxy myoglobin. *Nature 403*, 921–923.
23. Brunori, M., Vallone, B., Cutruzzola, F., Travaglini-Allocatelli, C., Berendzen, J., Chu, K., Sweet, R. M., and Schlichting, I. (2000) The role of cavities in protein dynamics: crystal structure of a photolytic intermediate of a mutant myoglobin. *Proc. Natl. Acad. Sci. U.S.A. 97*, 2058–2063.
24. Schotte, F., Lim, M., Jackson, T. A., Smirnov, A. V., Soman, J., Olson, J. S., Phillips, G. N., Jr., Wulff, M., and Anfinrud, P. A. (2003) Watching a protein as it functions with 150-ps time-resolved x-ray crystallography. *Science 300*, 1944–1947.
25. Hummer, G., Schotte, F., and Anfinrud, P. A. (2004) Unveiling functional protein motions with picosecond x-ray crystallography and molecular dynamics simulations. *Proc. Natl. Acad. Sci. U.S.A. 101*, 15330–15334.
26. Schmidt, M., Nienhaus, K., Pahl, R., Krasselt, A., Anderson, S., Parak, F., Nienhaus, G. U., and Srajer, V. (2005) Ligand migration pathway and protein dynamics in myoglobin: a time-resolved crystallographic study on L29W MbCO. *Proc. Natl. Acad. Sci. U.S.A. 102*, 11704–11709.
27. Nienhaus, K., Ostermann, A., Nienhaus, G. U., Parak, F. G., and Schmidt, M. (2005) Ligand migration and protein fluctuations in myoglobin mutant L29W. *Biochemistry 44*, 5095–5105.
28. Scott, E. E., and Gibson, Q. H. (1997) Ligand migration in sperm whale myoglobin. *Biochemistry 36*, 11909–11917.
29. Scott, E. E., Gibson, Q. H., and Olson, J. S. (2001) Mapping the pathways for O_2 entry into and exit from myoglobin. *J. Biol. Chem. 276*, 5177–5188.
30. Nienhaus, K., Deng, P., Belyea, J., Franzen, S., and Nienhaus, G. U. (2006) Spectroscopic study of substrate binding to the carbonmonoxy form of dehaloperoxidase from Amphitrite ornata. *J. Phys. Chem. B 110*, 13264–13276.
31. Kriegl, J. M., Nienhaus, K., Deng, P., Fuchs, J., and Nienhaus, G. U. (2003) Ligand dynamics in a protein internal cavity. *Proc. Natl. Acad. Sci. U.S.A. 100*, 7069–7074.
32. Lehle, H., Kriegl, J. M., Nienhaus, K., Deng, P., Fengler, S., and Nienhaus, G. U. (2005) Probing electric fields in protein cavities by using the vibrational stark effect of carbon monoxide. *Biophys. J. 88*, 1978–1990.
33. Nienhaus, K., Olson, J. S., Franzen, S., and Nienhaus, G. U. (2005) The origin of Stark splitting in the initial photoproduct state of MbCO. *J. Am. Chem. Soc. 127*, 40–41.
34. Franzen, S. (2002) An electrostatic model for the frequency shifts in the carbonmonoxy stretching band of myoglobin: Correlation of hydrogen bonding and the Stark tuning rate. *J. Am. Chem. Soc. 124*, 13271–13281.
35. Nienhaus, K., Deng, P., Olson, J. S., Warren, J. J., and Nienhaus, G. U. (2003) Structural dynamics of myoglobin: Ligand migration and binding in valine 68 mutants. *J. Biol. Chem. 278*, 42532–42544.
36. Mourant, J. R., Braunstein, D. P., Chu, K., Frauenfelder, H., Nienhaus, G. U., Ormos, P., and Young, R. D. (1993) Ligand binding to heme proteins: II. Transitions in the heme pocket of myoglobin. *Biophys. J. 65*, 1496–1507.
37. Nienhaus, K., and Nienhaus, G. U. (2008) Ligand dynamics in heme proteins observed by Fourier transform infrared spectroscopy at cryogenic temperatures. *Methods Enzymol. 437*, 347–378.
38. Henry, E. R., Sommer, J. H., Hofrichter, J., and Eaton, W. A. (1983) Geminate recombination of carbon monoxide to myoglobin. *J. Mol. Biol. 166*, 443–451.
39. Braunstein, D. P., Chu, K., Egeberg, K. D., Frauenfelder, H., Mourant, J. R., Nienhaus, G. U., Ormos, P., Sligar, S. G., Springer, B. A., and Young, R. D. (1993) Ligand binding to heme proteins: III. FTIR studies of His-E7 and Val-E11 mutants of carbonmonoxymyoglobin. *Biophys. J. 65*, 2447–2454.
40. Li, T., Quillin, M. L., Phillips, G. N., Jr., and Olson, J. S. (1994) Structural determinants of the stretching frequency of CO bound to myoglobin. *Biochemistry 33*, 1433–1446.
41. Ray, G. B., Li, X.-Y., Ibers, J. A., Sessler, J. L., and Spiro, G. S. (1994) How far can proteins bend the FeCO unit? *J. Am. Chem. Soc. 116*, 162–176.
42. Vogel, K. M., Kozlowski, P. M., Zgierski, M. Z., and Spiro, T. G. (1999) Determinants of the FeXO (X = C, N, O) vibrational frequencies in heme adducts from experiment and density functional theory. *J. Am. Chem. Soc. 121*, 9915–9921.
43. Phillips, G. N., Jr., Teodoro, M. L., Li, T., Smith, B., and Olson, J. S. (1999) Bound CO is a molecular probe of electrostatic potential in the distal pocket of myoglobin. *J. Phys. Chem. B 103*, 8817–8829.
44. Park, E. S., and Boxer, S. G. (2002) Origins of the sensitivity of molecular vibrations on electric fields: Carbonyl and nitrosyl stretches in model compounds and proteins. *J. Phys. Chem. 106*, 5800–5806.
45. Yang, F., and Phillips, G. N., Jr. (1996) Crystal structures of CO-, deoxy- and met-myoglobins at various pH values. *J. Mol. Biol. 256*, 762–774.
46. Vojtechovsky, J., Chu, K., Berendzen, J., Sweet, R. M., and Schlichting, I. (1999) Crystal structures of myoglobin-ligand complexes at near-atomic resolution. *Biophys. J. 77*, 2153–2174.
47. Alben, J. O., Beece, D., Bowne, S. F., Doster, W., Eisenstein, L., Frauenfelder, H., Good, D., McDonald, J. D., Marden, M. C., Moh, P. P., Reinisch, L., Reynolds, A. H., Shyamsunder, E., and Yue, K. T. (1982) Infrared spectroscopy of photodissociated carboxymyoglobin at low temperatures. *Proc. Natl. Acad. Sci. U.S.A. 79*, 3744–3748.
48. Young, R. D., Frauenfelder, H., Johnson, J. B., Lamb, D. C., Nienhaus, G. U., Phillip, R., and Scholl, R. (1991) Time- and temperature dependence of large-scale conformational transitions in myoglobin. *Chem. Phys. 158*, 315–328.
49. Müller, J. D., McMahon, B. H., Chien, E. Y., Sligar, S. G., and Nienhaus, G. U. (1999) Connection between the taxonomic substates and protonation of histidines 64 and 97 in carbonmonoxy myoglobin. *Biophys. J. 77*, 1036–1051.
50. Laurenti, E., Ghibaudi, E., Ardissone, S., and Ferrari, R. P. (2003) Oxidation of 2,4-dichlorophenol catalyzed by horseradish peroxidase: characterization of the reaction mechanism by UV-visible spectroscopy and mass spectrometry. *J. Inorg. Biochem. 95*, 171–176.
51. Nienhaus, G. U., Heinzl, J., Huenges, E., and Parak, F. (1989) Protein crystal dynamics studied by time-resolved analysis of x-ray diffuse scattering. *Nature 338*, 665–666.
52. Parak, F. G., and Nienhaus, G. U. (2002) Myoglobin, a paradigm in the study of protein dynamics. *ChemPhysChem 3*, 249–254.
53. Douzou, P. (1977) *Cryobiochemistry*, Academic Press, New York.
54. Lim, M., Jackson, T. A., and Anfinrud, P. A. (1997) Ultrafast rotation and trapping of carbon monoxide dissociated from myoglobin. *Nat. Struct. Biol. 4*, 209–214.
55. Nutt, D. R., and Meuwly, M. (2003) Theoretical investigation of infrared spectra and pocket dynamics of photodissociated carbonmonoxy myoglobin. *Biophys. J. 85*, 3612–3623.
56. Hartmann, H., Zinser, S., Komninos, P., Schneider, R. T., Nienhaus, G. U., and Parak, F. (1996) X-ray structure determination of a metastable state of carbonmonoxy myoglobin after photodissociation. *Proc. Natl. Acad. Sci. U.S.A. 93*, 7013–7016.

57. Schlichting, I., Berendzen, J., Phillips, G. N., Jr., and Sweet, R. M. (1994) Crystal structure of photolysed carbonmonoxy-myoglobin. *Nature 371*, 808–812.
58. Teng, T. Y., Srajer, V., and Moffat, K. (1994) Photolysis-induced structural changes in single crystals of carbonmonoxy myoglobin at 40 K. *Nat. Struct. Biol. 1*, 701–705.
59. Meuwly, M. (2006) On the influence of the local environment on the CO stretching frequencies in native myoglobin: assignment of the B-states in MbCO. *ChemPhysChem 7*, 2061–2063.
60. Bredenbeck, J., Helbing, J., Nienhaus, K., Nienhaus, G. U., and Hamm, P. (2007) Multidimensional ultrafast spectroscopy special feature: Protein ligand migration mapped by nonequilibrium 2D-IR exchange spectroscopy. *Proc. Natl. Acad. Sci. U.S.A. 104*, 14243–14248.
61. Johnson, J. B., Lamb, D. C., Frauenfelder, H., Müller, J. D., McMahon, B., Nienhaus, G. U., and Young, R. D. (1996) Ligand binding to heme proteins. VI. Interconversion of taxonomic substates in carbonmonoxymyoglobin. *Biophys. J. 71*, 1563–1573.
62. Nienhaus, G. U., Müller, J. D., McMahon, B. H., and Frauenfelder, H. (1997) Exploring the conformational energy landscape of proteins. *Physica D 107*, 297–311.
63. Rohlfs, R. J., Mathews, A. J., Carver, T. E., Olson, J. S., Springer, B. A., Egeberg, K. D., and Sligar, S. G. (1990) The effects of amino acid substitution at position E7 (residue 64) on the kinetics of ligand binding to sperm whale myoglobin. *J. Biol. Chem. 265*, 3168–3176.
64. Matsui, T., Ozaki, S., Liong, E., Phillips, G. N., Jr., and Watanabe, Y. (1999) Effects of the location of distal histidine in the reaction of myoglobin with hydrogen peroxide. *J. Biol. Chem. 274*, 2838–2844.

BI801564R